

## Effect of Sintering on Aeolian Snow Erosion

Abdou Khalil<sup>1,\*</sup>, Hervé Bellot<sup>2</sup>, Yoichi Ito<sup>3</sup>, Pascal Dupont<sup>1,4</sup>, Florence Naaim-Bouvet<sup>2</sup>, Ahmed Ould El Moctar<sup>5</sup>, and Alexandre Valance<sup>1</sup>

<sup>1</sup>IPR, Univ Rennes, CNRS UMR 6251, Campus Beaulieu, Rennes,F-35042, Bretagne, France

<sup>2</sup>Univ. Grenoble Alpes, IRD, CNRS, INRAE, Grenoble INP\*, IGE, Grenoble,F-38000, Auvergne Rhône-Alpes, France

<sup>3</sup>Snow and Ice Research Center, National Research Institute for Earth Science and Disaster Resilience, Nagaoka 940-0821, Japan

<sup>4</sup>LGCGM, INSA Rennes, Univ Rennes, Campus Beaulieu, Rennes,F-35000, Bretagne, France

<sup>5</sup>LTeN, Univ Nantes, UMR CNRS 6607, Rue Christian Pauc, Nantes,F-44306, Pays de la Loire, France

**Abstract.** The quantitative description of aeolian snow transport remains a challenging issue for theoretical modelling but also for environmental concerns. Drifting snow is crucially dependent on snow cover properties, including cohesive force and snow type. Snow transport is particularly impacted by cohesive processes in contrast to wind-blown sand. Our study explores in particular the effect of snow sintering on both the aerodynamic and impact erosion processes. We propose here an original experimental set-up to determine both the aerodynamic and impact erosion rate in the context of snow packs. The experiments were carried out in the cold wind-tunnel at the Cryospheric Environment simulator in Shinjo with snow packs of various sintering times. Our results reveal that as sintering time is increased, impact erosion efficiency—which is determined by the number of particles ejected per impact—is decreased. Our preliminary findings are in line with recent experiments made with moist sand, suggesting similarities between snow and moist sand.

### 1 Introduction

Aeolian transport of particles, including sand and snow, is a process that shapes natural landscapes and influences environmental systems. In cold regions, wind-driven snow transport affects environmental and infrastructural surroundings, influencing snow erosion, drifting and avalanche formation. Understanding the thresholds that initiate and sustain particle transport—the aerodynamic threshold and the impact threshold, respectively—is essential to predict these processes. These thresholds are governed by particle-fluid interactions, environmental factors and the cohesive properties of the particles which lack controlled experiments.

For non-cohesive materials, such as dry sand, the physical mechanisms governing aeolian transport processes have been widely studied during the past decades and are now relatively well understood [1–3]. Bagnold [4] established the principal foundation describing the dynamics of sand grain. In particular, he emphasized the important role of the erosion induced by the impact of saltating particles, the so-called splash process. In the context of non-cohesive granular materials the impact process has been thoroughly studied through model collision experiments [5–7] and numerical simulations [8, 9]. One of the remaining issue is to investigate how impact erosion is modified for cohesive materials like moist sand and snow.

Snow is a complex material regarding transport dynamics. Snow particles are irregular in shape and cohe-

sive, its transport is then highly sensitive to temperature and humidity. Indeed, snow cohesion could vary in time due to a process called sintering where ice bonds form between particles and generally increases through time as bonds continue to form.

There is a large gap regarding the influence of sintering on the snow transport properties. Very few experimental studies report on the splash process with cohesive granular packing. In contrast, numerical studies were recently developed. Comola et al. [10] developed a 3D discrete element method (DEM) for investigated the erosion of a granular packing made cohesive with icy bonds. Ralarisoa et al [11] studied again via DEM the splash process with a cohesive granular packing made cohesive with liquid bridges. These studies suggest that the impact erosion process exhibits different features according to the level of cohesion. Three regimes were identified. For weak cohesion, the ejection of particles is not altered by the presence of cohesive bonds. For intermediate cohesion, the erosion efficiency decreases while the critical impact velocity to trigger the splash process remains unchanged in comparison with the cohesionless case. For higher cohesion, the critical impact velocity increases while the erosion efficiency keeps decreasing. These outcomes are summarized in Fig. 1, where the number of ejected particles per impact,  $N_e$ , is plotted as a function of the dimensionless impact velocity  $V_i/V_{ic} - 1$  for different cohesion numbers  $Co^*$  ( $Co^* = W_c/P$  defined as the ratio of the energy needed to break a cohesive bond  $W_c$  to the grain weight  $P$  and  $V_{ic}$  is the critical impact velocity below which there is no ejection).

\*e-mail: [abdou.khalil@univ-rennes.fr](mailto:abdou.khalil@univ-rennes.fr)

tion in a cohesionless case). Selmani et al. [12] showed that the critical cohesion numbers that define the regime transitions in [10] are  $Co_1^* \approx 0.1$  and  $Co_2^* \approx 2$  for cohesive beds with ice bridges. Both moist sand and snow show similar behaviors. These numerical outcomes have been recently confirmed by experiments made with cohesive sand [12, 13].

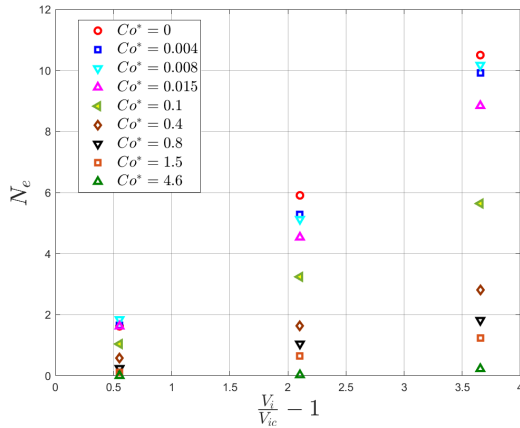


**Figure 1.** Number of ejected particles per impact  $N_e$  as a function of the dimensionless impact velocity  $V_i/V_{ic} - 1$  for different cohesion number  $Co^*$  (Data from [10] extracted from Selmani et al.[12]).

The challenge of the present work is to investigate experimentally the effect of snow sintering on the splash process. We used a similar approach as that used by Besnard et al. for cohesive sands [12, 13]. The experiments were carried out in a cold wind tunnel at the Cryospheric Environment Simulator [14]. Various snow samples were studied and the cohesion strength was varied by increasing the sintering time. Preliminary results are promising for a first experimental characterization of the splash process in the context of snow.

## 2 Experimental Setup and Calibration

### 2.1 Wind-tunnel Facility

The experiments were conducted in a closed-loop wind tunnel (Figure 2) with a test section that measures 14 meters in length and has a cross-section of  $1m \times 1m$ . A fan generates an airflow within the tunnel at a nominal speed  $U_\infty$ , corresponding to the reference velocity measured using a Pitot tube placed 14 cm below the ceiling, upstream of the test section. The wind speed can be varied from 0 to 20 m/s. The average temperature is  $T = -10^\circ C$  and the mean relative humidity of the air is  $HR = 82\%$ . The floor of the tunnel is covered by a non-erodible icy bed obtained by spraying water over an artificial snow layer. The turbulent air flow was characterized by 3D ultrasonic anemometers and the velocity profile was found to obey the classical logarithmic law of the wall given by:

$$U(z) = \frac{u^*}{\kappa} \ln\left(\frac{z}{z_0}\right) \quad (1)$$

where  $u^*$  is the so-called friction velocity,  $z_0$  is the aerodynamic roughness length and  $\kappa = 0.41$  is the Von Karman

constant. The friction velocity  $u^*$  was found to be proportional to the nominal flow velocity  $U_\infty$  ( $u^* \approx 0.037 U_\infty$ ) and  $z_0$  is roughly constant and equal to  $z_0 \approx 2 \times 10^{-5}m$ ; These characteristics are specific to the wind-tunnel and the iced floor.

### 2.2 Seeding system

A seeding system is set at the beginning of the test section and allows to feed the turbulent air flow with an incoming mass flux  $Q_{in}$  of snow. The seeder is filled with artificial snow (see next subsection for further details) which goes through a sieve of  $500 \mu m$ . The incoming mass flux can be assessed via a snow particle counter (SPC-S7) [14] which is positioned downstream in the center of the tunnel.

The Snow Particle Counter (SPC) is an optical sensor that measures airborne particle transport by detecting the shadows cast as particles cross a  $2 \times 25 \text{ mm}^2$ , 0.5 mm thick laser beam. It provides data on particle size distribution and horizontal flux density at a specific height (Fig. 3). SPC was used to measure accurately the incoming mass flux  $Q_{in}$  which could vary from one experiment to another due to clogging issues of the sieve of the seeding system.

The SPC measurements provided us with an estimate of the median diameter  $d$  of the particle coming from the seeder:  $d \approx 250 \mu m$ .

### 2.3 Snow Samples

The snow samples under study are placed downstream at a position  $x = 12.6 m$  from the beginning of the test section. They are displayed in a square box with a side of 20 cm and a depth of 2 cm. They are subject either to the aerodynamic erosion from the shearing of a clear turbulent air flow or by the erosion induced by the impact of the particles coming from the seeder.

The snow under study is artificial snow produced at the facility by the NIED snowfall machine [14]. The box was filled on average with 210 g of snow (corresponding to a constant volume fraction of 0.28). The filling was achieved using a  $500 \mu m$  sieve. Once filled up, the surface of the snow pack was leveled off using a ruler. The waiting time between the preparation of the sample and the experiment was varied between 0 and 900 minutes to study the effect of sintering. We studied four different samples with sintering times 0, 60, 120 and 900 minutes.

### 2.4 Experimental protocol

At the beginning of an experiment, the snow sample is weighed. The sample is placed in the tunnel and is then subject to either aerodynamic or impact erosion for a finite time. At the end of the experiment, the sample is again weighed. From the mass loss, we can calculate the erosion rate  $E$ :

$$E = -\frac{M_f - M_i}{S \times T} \quad (2)$$

where  $M_i$  and  $M_f$  are the initial and final mass of the sample,  $S = 4.10^{-2} m^2$  the surface area of the box and  $T$  the duration of the experiment.

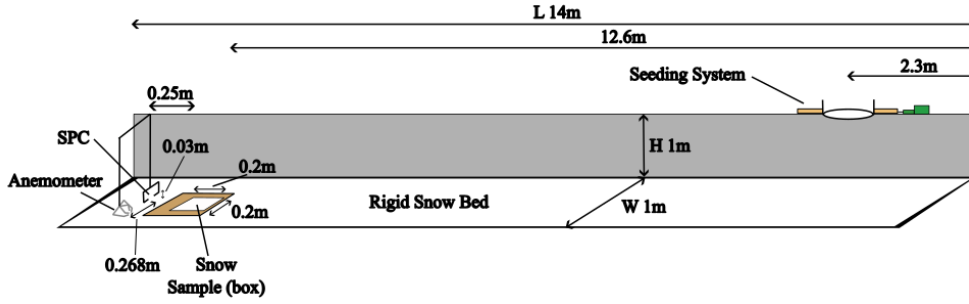


**Figure 2.** Illustration of the test section of the climatic wind tunnel in Japan. The air flow will be moving from right to left. At 2.3m downstream from the tunnel entrance we have a seeding system to introduce an upstream mass flux of snow. The snow sample is confined in a 20cm x 20cm x 2cm box and placed at 12.6m downstream. While, an SPC and a 3D ultrasonic anemometer are positioned 13.05m downstream. The SPC is placed along the centerline of the tunnel, while the anemometer is offset 26.8cm to the left of the centerline.

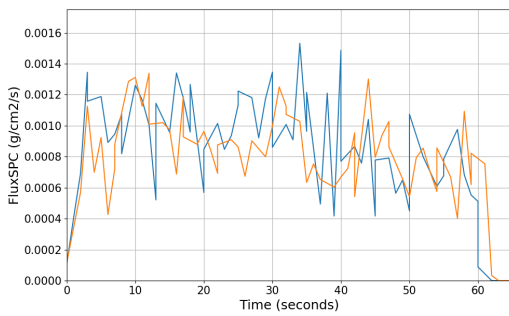


**Figure 3.** The incoming mass flux density as a function of time for two experiments with the nominal velocity  $U_\infty = 6\text{m/s}$ .

### 3 Aerodynamic erosion

The experiments carried out for characterizing the aerodynamic erosion were not successful. Indeed, the turbulent air flow achieved with the maximum power of the fans and providing a nominal velocity  $U_\infty = 20\text{m/s}$  was not able to erode any of the snow samples, even the one with the smallest sintering time meaning the aerodynamic threshold for all samples is higher than  $u^* \approx 0.74\text{m/s}$ . Typical aerodynamic threshold velocities reported for a similar setup is  $0.3\text{ m/s}$  (Besnard et al.[13]) for dry cohesionless sand of  $200\ \mu\text{m}$ . Our outcome thus shows the high cohesion of sintered snow.

### 4 Impact erosion

The impact erosion rate is expected to be proportional to the impact flux  $\phi$  and can be expressed as:

$$E = \phi \times N_e(V_i, Co^*, \dots) \quad (3)$$

where the average number of ejected particles per impact  $N_e$  depends on the impact velocity  $V_i$  and the cohesion number  $Co^*$ .

Our goal is to evaluate the variation of  $N_e$  with  $V_i$  and  $Co^*$ . Cohesion is varied by increasing the sintering time  $t_s$  while impact velocity  $V_i$  is controlled by the wind strength. The exact relationships between  $Co^*$  and  $t_s$ , and between  $V_i$  and  $u^*$ , have not yet been established. Further experiments are planned to investigate the variation of cohesion strength with sintering time using micro-mechanical tests, and to assess the velocity of impacting particles through imaging techniques. As emphasized by Eq. 3, the evaluation of  $N_e$  requires the knowledge of the impact flux  $\phi$

which varies with the wind speed for a given incoming mass flux  $Q_{in}$ .

#### 4.1 Measurement of $\phi$

The impact flux  $\phi$  is obtained directly by trapping the impacting particles at the location of the snow box. To trap the snow particles, we replaced the snow sample with silicon oil to efficiently trap the particles.  $\phi$  was then estimated by weighing method as for the erosion rate. [12, 13].

We thus characterized the dependence of  $\phi$  with the friction velocity  $u^*$  (see Fig 4). The data indicate that  $\phi$  fit the law observed by [13] and is very well captured by:

$$\phi = Q_{in} \frac{Ag}{(u^* - u_{reb}^*)^2} \quad (4)$$

where  $A$  a fit parameter ( $A \approx 1/250$ ),  $g$  the gravitational acceleration ( $g = 9.81\text{m/s}^2$ ) and  $u_{reb}^*$  the critical shear velocity to sustain the motion of a single particle on the rigid icy bed ( $u_{reb}^* \approx 0.06\text{m/s}$ ).

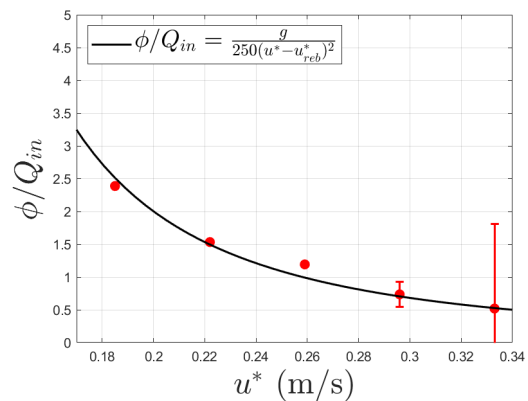


**Figure 4.** Rescaled impact flux  $\phi/Q_{in}$  as a function of the friction velocity  $u^*$ .

#### 4.2 Measurement of the rescaled erosion $E/\phi$

We provide here preliminary results of the rescaled erosion rate  $E/\phi$  as a function of the sintering time for a given friction velocity (see Fig. 5).  $E/\phi$  can be interpreted as the number of ejected particles per impact  $N_e$ . This indicates that the impact erosion process is less and less efficient as the sintering time and the cohesion are increased.

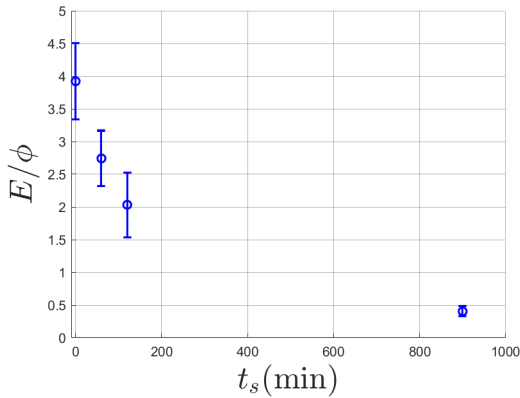


**Figure 5.** Rescaled erosion rate  $E/\phi$  as a function of the sintering time  $t_s$  for a friction velocity ( $u^* \approx 0.29\text{m/s}$ )

We are currently investigating the impact erosion process over a wide range of friction velocities to have a complete description of  $E/\phi$  as a function of the sintering time  $t_s$  and the friction velocity  $u^*$  to be able to compare our experimental data to the numerical ones of [10, 11].

## 5 Discussion and conclusion

Similar wind tunnel experiments were carried out with cohesive sand [12, 13] but never with snow. These experiments are the first to characterize the erosion process by impact on snow.

The main issue is to determine whether the erosion mechanisms differ for cohesive sand where cohesion is ensured by capillary bridge and snow where the bonds are formed by solid ice bridge. Numerical simulations done on particle impact on cohesive granular packings in the context of liquid bridges [11] and solid bridges [10] indicate that the process of impact erosion is similar. The completion of our experiments should provide a definite answer.

The remaining issue is to quantify the cohesion strength of our snow sample as a function of the sintering time. One method to do it is to estimate the minimum friction speed at which the snow starts to be eroded aerodynamically. Unfortunately, this method is not effective because it requires wind speeds that are inaccessible to our wind tunnel. An alternative method is based on classical mechanical tests using a snow micro-penetrometer. Preliminary estimates of this cohesive force are in the order of  $400 \mu\text{N}$  for  $t_s = 0$  min and  $1700 \mu\text{N}$  for  $t_s = 60$  min.

These results indicate that, despite snow's high cohesiveness, erosion occurred primarily through particle impact rather than aerodynamic entrainment, suggesting that impact is the dominant mechanism governing snow erosion. Further research into this process is crucial for improving the accuracy of snow transport models.

## Acknowledgements

We thank Dr. Housseem Selmani for his analytical assistance, the French Research National Agency (Project No. ANR-21-CE30-0066) for funding, and NIED, along with Cryospheric Environmental Simulator staff Kazuma To-

gashi, Genzo Okawa, and Koichi Suzuki, for experimental support.

## References

- [1] J.F. Kok, N.O. Renno, A comprehensive numerical model of steady state saltation (COMSALT), *Journal of Geophysical Research: Atmospheres* **114** (2009). <https://doi.org/10.1029/2009JD011702>
- [2] O. Durán, P. Claudin, B. Andreotti, On aeolian transport: Grain-scale interactions, dynamical mechanisms and scaling laws, *Aeolian Research* **3**, 243 (2011). [10.1016/j.aeolia.2011.07.006](https://doi.org/10.1016/j.aeolia.2011.07.006)
- [3] A. Valance, K.R. Rasmussen, A. Ould El Moctar, P. Dupont, The physics of Aeolian sand transport, *Comptes Rendus. Physique* **16**, 105 (2015). [10.1016/j.crhy.2015.01.006](https://doi.org/10.1016/j.crhy.2015.01.006)
- [4] R.A. Bagnold, in *The Physics of Blown Sand and Desert Dunes* (Springer Netherlands, Dordrecht, 1941), pp. 57–76
- [5] M. Ammi, L. Oger, D. Beladjine, A. Valance, Three-dimensional analysis of grain ejection by an impacting bead, *Physical Review E* **79**, 021305 (2009).
- [6] D. Beladjine, M. Ammi, L. Oger, A. Valance, Collision process between an incident bead and a three-dimensional granular packing, *Physical Review E* **75**, 061305 (2007).
- [7] S. Mitha, M.Q. Tran, B.T. Werner, P.K. Haff, The dynamics of aeolian sand transport, *Acta Mechanica* **63**, 267 (1986).
- [8] L. Oger, M. Ammi, A. Valance, D. Beladjine, Study of the rebound of solid particles: Application to aeolian transport, *European Physical Journal E* **17**, 467 (2005).
- [9] R.S. Anderson, P.K. Haff, in *Aeolian Grain Transport I*, edited by O.E. Barndorff-Nielsen, B.B. Willetts (Springer Vienna, Vienna, Vienna, 1991), Vol. 1, pp. 21–51
- [10] F. Comola, J. Gaume, J.F. Kok, M. Lehning, Cohesion-Induced Enhancement of Aeolian Saltation, *Geophysical Research Letters* **46**, 5566 (2019). <https://doi.org/10.1029/2019GL082195>
- [11] V. Ralaiarisoa, P. Dupont, A.O.E. Moctar, F. Naaim-Bouvet, L. Oger, A. Valance, Particle impact on a cohesive granular media, *Physical Review E* **105**, 054902 (2022). [10.1103/PhysRevE.105.054902](https://doi.org/10.1103/PhysRevE.105.054902)
- [12] H. Selmani, J.B. Besnard, A. Ould El Moctar, P. Dupont, A. Valance, Experimental study of particle impact on cohesive granular packing, *Physical Review E* **110**, 014901 (2024). [10.1103/PhysRevE.110.014901](https://doi.org/10.1103/PhysRevE.110.014901)
- [13] J. Besnard, P. Dupont, A.O. El Moctar, A. Valance, Aeolian Erosion Thresholds for Cohesive Sand, *Journal of Geophysical Research: Earth Surface* **127**, e2022JF006803 (2022). [10.1029/2022JF006803](https://doi.org/10.1029/2022JF006803)
- [14] T. Sato, K. Kosugi, A. Sato, Saltation-layer structure of drifting snow observed in wind tunnel, *Annals of Glaciology* **32**, 203 (2001). [10.3189/172756401781819184](https://doi.org/10.3189/172756401781819184)